# Evolution of deghosting process for single sensor streamer data from 2D to 3D

Zhigang Zhang*, Hassan Masoomzadeh, and Bin Wang

TGS-NOPEC Geophysical Company

*E-mail: Zhigang.zhang@tgs.com



This article has been accepted for publication and undergone full peer review but has not been through the copyediting, typesetting, pagination and proofreading process, which may lead to differences between this version and the Version of Record. Please cite this article as doi: 10.1111/gpr.12614

**Abstract**

In marine acquisition, reflections of sound energy from the water-air interface result in ghosts in the seismic data, both in the source side and receiver side. Ghosts limit the bandwidth of the useful signal and blur the final image. The process to separate the ghost and primary signals, called the deghosting process, can fill the ghost notch, broaden the frequency band, and help to achieve high-resolution images. Low signal to noise ratio near the notch frequencies and 3D effects are two challenges that the deghosting process has to face. In this paper, starting from an introduction to the deghosting process, we present and compare two strategies to solve the latter. The first is an adaptive mechanism which adjusts the deghosting operator to compensate for 3D effects or errors in source/receiver depth measurement. This method does not include explicitly the crossline slowness component and is not affected by the sparse sampling in the same direction. The second method is an inversion type approach which does include the crossline slowness component in the algorithm and handles the 3D effects explicitly. Both synthetic and field data examples in wide azimuth (WAZ) acquisition settings are shown to compare the two strategies. Both methods provide satisfactory results.

**Keywords:** Data processing, Noise, Signal processing, Deghosting

## Introduction

The frequency bandwidth of usable signal in marine seismic acquisition used to be limited by ghosts from both source and receiver sides, caused by reflections of sound waves from the water-air interface. The interference between the up-going and down-going wave is constructive for some frequencies while destructive for some others. At the notch frequency, the destructive effect could be so strong that little or no signal energy remains. The deghosting process de-convolves the ghost effect from the acquired data, recovers the lost signal near those notch frequencies, broadens the signal spectrum, and helps to achieve high-resolution images (Monk and Byerley 2016).

Several hardware solutions are available now to alleviate the difficulties met in the deghosting stage. Since the particle velocity component has different ghost notches from the pressure component, multi-component streamers are designed to combine pressure and particle velocity or acceleration measurements to eliminate ghosts for the receiver side (Carlson *et al.* 2007; Ozbek *et al.* 2010). As ghost notches directly depend on receiver or source depth, allowing the source or receiver depths to change brings extra flexibility to diversify the ghost notches. Soubaras (2012) proposed the use of variable depth streamers. Dual-cable configuration is another example which utilizes two different receiver depths to improve the signal to noise ratio near the receiver side notch frequencies (Posthumus 1993; Ozdemir *et al.* 2008). Similarly, for the source side, air guns can be arranged at different depths to help the deghosting procedure.

However, legacy data is mostly acquired with pressure-only streamers towed at a constant depth, which is also still the case for many current acquisitions. Research on processing-based deghosting solutions for such “standard acquisition” has a long history (Jovanovich, Sumner, and Akins-Easterlin 1983). However, applications in production were quite limited until recent years when significant progress has been made in both acquisition and processing methods. During the past decade, this topic has attracted more attention as more and more computation power becomes available, also being driven by the ever-increasing requirement for high-resolution images from the industry (Zhou *et al.* 2012; Masoomzadeh and Woodburn 2013; Telling *et al.* 2014). The processing-based methods mostly work in the frequency domain and apply plane wave decomposition directly or indirectly, and these methods are the main topic of this paper. There are exceptions though. For example, Berkhout and Blacquiere (2015) proposed to treat the deghosting as an echo-blending problem, in which a ghost model is built and adaptively subtracted from the input data. Moreover, a time domain method predicting a ghost model using wave propagation and subtracting it from the input data has also been investigated (Robertsson and Amundsen 2014).

Accurate knowledge of the time gap between the primary and ghost is essential for any successful processing-based deghosting algorithms. In turn, plane wave decomposition, such as the linear Radon transformation, plays a critical role in many algorithms. The way in which this decomposition is used divides this set of algorithms into two categories. Consider the linear Radon transformation in frequency-slowness domain (f-$p_x$-$p_y$) for example. In the first category, the linear Radon transformation is applied on common shot gathers for receiver side deghosting or common receiver gathers for source side deghosting, followed by deghosting in the frequency-slowness domain. The deghosted data in the frequency-slowness domain then is transformed back into the time-offset (t-x-y) domain. Since linear Radon transformation is a mature technology and has been used by the industry for many years, this method is a popular choice (Zhou *et al.* 2012; Masoomzadeh and Woodburn 2013; Telling *et al.* 2014; Zhang *et al.* 2015). This set of algorithms works for streamers towed at constant depth.

The second category of processing-based methods based on plane wave decomposition does not utilize the transformations directly. Instead, the input data in the time-offset (t-x-y) domain is connected with its plane-wave decomposition, which may be in the frequency-slowness domain for example, by a transform matrix. The matrix combines the inverse linear Radon transformation operator, the ghosting operator, and possibly a re-datuming operator. A linear solver is then used to find the solution, which can be transformed back to the ghost-free data via an inverse linear Radon operator (Poole 2013; Wang, Ray, and Nimsaila 2014). This method requires accurate receiver and/or source depths and can be used for both fixed-depth and variable-depth streamers. When the recorded receiver or source depth is not reliable, algorithms have been designed to find a more accurate estimation (Hardwick *et al.* 2015; King and Poole 2015). This technique is also known as the inversion method.

In this paper, we choose the frequency-slowness domain for deghosting, but it is worth noting that the frequency-wavenumber domain provides an alternative type of plane wave decomposition from the frequency-slowness domain we use. Similarly, the frequency-wavenumber decomposition can be applied directly, as in the first category of algorithms mentioned (Amundsen 1992), or indirectly as in the latter (Riyanti *et al.* 2014).

In marine acquisition, the relatively dense sampling in the inline direction makes the linear Radon transformation in that direction feasible. However, the sparse spatial sampling in the crossline direction poses great challenges to deghosting, as it does to the Radon transformation. The difficulty to accomplish a true 3D transformation forces one to imply 2D assumptions in many practical applications. The unaccounted 3D effects, including side reflections, may cause artifacts such as ringing in the deghosted data. This difficulty may be addressed in various ways. One strategy is to divide data into small windows and use an adaptive deghosting mechanism which searches for optimal ghost delay times within each window. This makes the deghosting operator both time- and space-variant. This strategy can be combined with the linear Radon transformation if needed. In this paper, we refer to this method as the implicit 3D method since slowness in the crossline direction is not explicitly introduced into the algorithm. The second strategy for consideration belongs to the latter category of deghosting methods. It takes advantage of the sparseness constraint to shrink the range of slowness, especially in the crossline direction. The sparseness constraint reduces the number of unknowns and mitigates the aliasing problem (Wang *et al.* 2014). We refer to this method as the explicit 3D method as it explicitly accounts for the crossline slowness.

In this paper, we first introduce the deghosting operator we will use in a 2D setting. Then both the implicit and explicit 3D methods are presented with a synthetic example. Finally, field data examples are used to compare the two methods to show their advantages and drawbacks.

**Ghosting and deghosting operators, 2D deghosting methods**

The ghost always follows its primary with a time delay, called the ghost delay time. To simplify the problem, we only include one ghost operator in our discussion, because both source and receiver ghosts have the same form. In the frequency domain, we can write the ghosting operator for pressure signal as

$$g(f) = 1 - r(f)e^{-i\omega\Delta_{real}}, \quad (1)$$

where $\Delta_{real}$ is the real ghost delay time, $\omega = 2\pi f$, and $r(f)$ is the reflection coefficient at the sea surface.

For a calm sea surface, the reflection coefficient is close to 1 theoretically. In practice, wind-driven waves cause rough sea surface conditions, leading to scattering of the sound wave. This scattering is stronger for higher frequencies and changes with the direction in which the waves hit the sea surface. In turn, the reflection coefficient decreases with frequency. Both numerical simulation and theoretical analysis have been utilized to find a better estimate of the reflection coefficient in terms of the wave height and incident angle (Jovanovich *et al.* 1983; Orji, Sollner, and UiO 2013). In this paper, we ignore the effect of the incident angle and choose $r(f)$ as

$$r(f) = r_0 e^{-\frac{1}{\sigma^2}f^2}, \quad (2)$$

where σ is a positive parameter which determines how fast the reflection coefficient decreases with frequency, and $r_0$ is the reflection coefficient at zero Hz. The effect of wave height is included in the parameter σ. In practice, $r_0$ and σ are picked by experience and tuned by checking the deghosting result.

The constructive and destructive effects caused by the ghost can be seen in the ghosting operator's amplitude spectrum, presented in Figure 1a. At frequencies $f = k/\Delta_{real}$, where $k$ is any non-negative integer, primary and ghost energies cancel each other maximally. These frequencies are called the ghost notch frequencies. The deghosting operator, which deconvolves the ghost effect, is the reciprocal of the ghosting operator applied in frequency domain,

$$u(f) = \frac{1}{1-r(f)e^{-i\omega\Delta_{used}}}, \tag{3}$$

where $\Delta_{used}$ is the actual ghost delay time used in deghosting. If the reflection coefficient is 1 for all frequencies, the deghosting operator is unstable and singular at notch frequencies. A reasonably smaller reflection coefficient, or the one given by equation (2), makes the deghosting operator stable. Fortunately, differences caused by using a more practical reflection coefficient are mostly small, and only become obvious near the notch frequencies, as shown in Figure 1c and 1d. Moreover, a stabilized version of equation (3) is often used in practice as

$$u(f) = \frac{1-r(f)e^{i\omega\Delta_{used}}}{\left\|1-r(f)e^{-i\omega\Delta_{used}}\right\|^2+\alpha^2}, \tag{4}$$

where $\alpha$ is a small number to avoid division by zero. The amplitude of the operator is also limited to reduce artifacts.

The amplification effect of the deghosting operator could be significant near the notch frequencies, depending on the reflection coefficient used. Finding the right notch frequencies or the ghost delay time is critical for deghosting. The ghost delay time is known to be a function of the sound velocity $v$, the receiver or source depth $d$, and the incident angle $\theta$, as shown in Figure 2a. In the 2D case, let $p_x$ be the inline slowness, it is connected to the incident angle by $p_x = \frac{1}{v}\sin(\theta)$. Here we assume everything is in a 2D plane along the inline direction, including the incident angle. The delay time is then given to be

$$\Delta_{real} = \frac{2d}{v}\cos(\theta) = 2d\,\frac{\sqrt{1-{p_x}^2 v^2}}{v}. \quad (5)$$

When the spatial sampling in the inline direction is dense enough, $p_x$ could be extracted from the data after plane wave decomposition, and the deghosting could be realized in the frequency-slowness domain using equations (4) and (5) . This is called the 2D method. As shown in Figure 2b, the relation between the ghost delay time and $p_x$ is not linear. For example, when the incident angle changes from vertical ($p_x$=0 s/m) to 20$^o$ ($p_x$=0.000228 s/m when sound velocity equals 1500 m/s), the ghost delay time only changes about 6 percent.

This 2D assumption works relatively successfully for deep water and narrow azimuth (NAZ) acquisitions when the 3D effect is not significant (Masoomzadeh and Woodburn 2013). Because of the important role of the linear Radon transformation in this 2D deghosting algorithm, any effort to reduce errors and improve the focusing of energy is helpful. High-resolution transformations usually behave better than the regular or slant stacking algorithm. Using the real offset between source and receiver without assuming the receivers are uniformly distributed in a line may improve the result with possibly substantial differences. Masoomzadeh and Hardwick (2016) presented a nice comparison of different Radon transformations.

## The ghost delay time in a 3D setting

There are situations where the 2D assumption breaks down and the 3D effect is not negligible. When this happens, the incident angle is not aligned in the inline plane, and equation (5) only provides an upper limit since the real delay time reads

$$\Delta_{real} = 2d\,\frac{\sqrt{1-p_x{}^2v^2-p_y{}^2v^2}}{v}, \tag{6}$$

where $p_y$ represents the crossline slowness components, and all other variables are defined as before.

Ideally, the sampling in both inline and crossline directions is dense enough, and both $p_x$ and $p_y$ could be extracted from the data after a plane wave decomposition followed by deghosting. However, in marine acquisition streamers are often separated by 75 m to 150 m for a typical acquisition. The sparse sampling in the crossline direction causes aliasing and basically inhibits the direct extension of the 2D method into 3D in practice. In the following sections, we will present two strategies to overcome the challenges posed by the crossline sparse sampling.

## Implicit 3D algorithm

Instead of virtually applying the 3D plane wave decomposition involving both the inline and crossline slowness and dealing with strong aliasing, an alternative processing solution is to design an adaptive deghosting algorithm. This algorithm is both time- and space-variant (Rickett *et al.* 2014; Zhang *et al.* 2015) and avoids the difficulty of calculating the crossline slowness component.

The implicit algorithm separates data into overlapping small windows in both time and space or time and slowness directions, depending on the chosen domain, and it assumes small variance of ghost delay time in each window. Different deghosting operators are chosen for each window, and the 3D effect is taken into account by a delay time search engine.

The success of the implicit algorithm depends on how well events with different ghost delay times are separated. Its use is not limited to the slowness domain. The linear Radon transformation is optional, but it is recommended. The plane wave decomposition in the inline direction can separate crossing events, such as the multiples and primaries, and is usually quite reliable because of the dense sampling in the inline direction.

With fixed reflection coefficient, the ghost delay time is the only unknown parameter in the deghosting operator. It combines the source or receiver depth, the incident angle, and the sound velocity in water. The criterion, or the objective function used in searching the ghost delay time, is core to the implicit algorithm. For large windows, statistical quantities such as amplitude spectrum, phase spectrum, or autocorrelation work well. Unfortunately, the adaptive algorithm mostly uses smaller windows and there are often not enough data to average out geological effects or noise.

Consider the obtained deghosted data, denoted as $p_{dg}(f)$, which can be written in the frequency domain as

$$p_{dg}(f) = u(f)g(f)p(f) = \frac{1-r(f)e^{-i\omega\Delta_{real}}}{1-r(f)e^{-i\omega\Delta_{used}}}p(f), \tag{7}$$

where $p(f)$ is the true primary without ghost, and all other variables are defined as before. Incorrectly selected ghost delay time causes over boosting of energy at the wrong notch frequencies and ringing in the time domain. Thus, the L1 norm or L2 norm of the deghosted data can be used as a criterion in the searching (Rickett *et al.* 2014). Kurtosis is another reported functional statistical measure (Grion, Telling, and Barnes 2015), defined as $k(x) = \frac{E[(x-\eta)^4]}{(E[(x-\eta)^2])^2}$, where $\eta$ is the mean of $x$. Different from the L1 norm or L2 norm, kurtosis is assumed to achieve its maximum at the right ghost delay time. We found that the L1 norm behaves more robustly than either the kurtosis or the L2 norm in many field data tests. It is also easier to calculate. A global search is applied to make sure that the search will not end in a local minimum, such as half of the real delay time. When knowledge about $\Delta_{real}$ is available, such as a better estimation of the range of ghost delay time, it can be applied as a constraint in the computation. Including the prior knowledge stabilizes the search, makes it robust to noise, and reduces computation time.

**Explicit 3D deghosting algorithm**

If aliasing effects are accounted for, the crossline slowness component $p_y$ could be explicitly included in the linear Radon transformation as its inline counterpart in a least-square type solution. This method enables deghosting for slanted streamers, since individual receiver depth can be naturally included in the transformation equations. The least-square solvers can also take advantage of high-resolution techniques such as reweighting (Trad, Ulrych, and Sacchi 2003). The set of equations is built up in terms of the plane wave decomposition of the up-going field at a certain datum, typically the water surface, and solved using the preconditioned conjugate gradient method.

At the angular frequency $\omega$, the input data at a certain receiver reads

$$d(x_i,\ y_i, \omega) = \sum_{m=1}^{npx} \sum_{n=1}^{npy} m\left(p_{x,m}, p_{y,n}, \omega\right) \times e^{-i\omega\left(p_{x,m}x_i + p_{y,n}y_i\right)}\left(e^{i\omega p_{z,m,n}z_i} - r(f)e^{-i\omega p_{z,m,n}z_i}\right) \tag{8}$$

where $d(x_i,\ y_i, w)$ is the Fourier transformation of the input data, $x_i,\ y_i$, and $z_i$ are the x coordinate, y coordinate, and depth of the i$^{\text{th}}$ receiver, respectively, $m\left(p_{x,m}, p_{y,n}, \omega\right)$ is the Fourier transformation of $p_{x,m}, p_{y,n}$ components of the upgoing wave field at the sea surface, and $npx$ and $npy$ are the number of $p_{x,m}$ and $p_{y,n}$, respectively. The vertical slowness component $p_{z,m,n} = \sqrt{\frac{1}{v^2} - {p_{x,m}}^2 - {p_{y,n}}^2}$. This set of equations is mostly under-determined. Therefore, we find the solution by minimizing an objective function defined as

$$\|\boldsymbol{d} - \boldsymbol{Am}\|_{L2} + \varepsilon\|\boldsymbol{Wm}\|_{L2}\ , \tag{9}$$

where $\boldsymbol{d} = \{d(x_i,\ y_i, \omega)\}$, $\boldsymbol{m} = \{m\left(p_{x,m}, p_{y,n}, \omega\right)\}$, $\boldsymbol{W}$ is a weight matrix, and $\boldsymbol{A}$ is the corresponding transformation operator, which combines the re-datuming operator, the ghosting operator, and the inverse linear Radon transformation operator. Parameter $\varepsilon$ balances the fitting error and the amplitude of the solution. This algorithm can achieve deghosting and redatuming at the same time.

Aliasing from the sparse sampling in the crossline direction is a large concern to the explicit 3D deghosting algorithm. The sampling rate in the space domain determines the frequency where aliasing becomes a serious issue for the linear Radon transformation. In marine acquisition, sampling is extremely unbalanced between the inline and crossline direction. While receiver spacing along the streamer is about 6.5 m to 12.5 m, the separation between neighboring streamers could be beyond 150 m. For regularized sampling, aliasing starts to appear at the frequency

$$f_a = \frac{1}{\Delta x(p^{max} - p^{min})}, \tag{10}$$

where $\Delta x$ is the sampling distance, and $p^{max}$ and $p^{min}$ are the possible maximum and minimum slownesses in the corresponding direction, respectively. For 100 m separated streamers and 1500 m/s sound velocity, the aliasing frequency is 7.5 Hz if $p_y$ ranges through all feasible values. This is far below the desired frequency bound.

If we can shrink the size of the feasible domain of $p_x$ and $p_y$, we can lift the aliasing frequency and reduce the artifacts. Considering the feasible domain of $p_x$ and $p_y$ of a general shot gather with several streamers, it is only limited by the sound velocity in water. However, the effective range of slowness will be much smaller if constrained into small cubes which consist of only a few streamers, a subset of receivers with a short record length.

The explicit 3D algorithm separates a common shot or receiver gather into overlapping cubes, and realizes deghosting in each cube in two steps, or two runs. For the first run, equations (8) are solved using all possible $p_x$ and $p_y$ for low frequencies before aliasing becomes a concern. The solution can then be used to define an effective set of $p_x$ and $p_y$, while other unknowns are assumed to be zero. The second run solves the equations (8) again but only involving the slowness pairs picked after the first run, which is a much smaller set. The reweighting technique can be used in the second run to further reduce possible aliasing (Wang *et al.* 2014), or in the first run to improve the resolution. To reduce the risk of missing weak events, this process can be repeated several times, called iterations. In each iteration, the algorithm is applied on the residue from the previous iteration.

**Synthetic WAZ data example**

In the case of WAZ acquisition, the 2D assumption is broken and 3D effects cannot be neglected. The crossline slowness is not always zero, and it changes along offset and time. To compare different algorithms, we made a simple synthetic example using the finite difference method. The model we used includes 3 layers of flat reflectors, located at 600 m, 1600 m, and 2600 m, respectively. The sound velocity above the first reflector is constantly 1500 m/s and linearly increases to 4000 m/s at 4000 m depth. Nine streamers are towed 50 m below the water surface, and the center streamer is 1500 m away from the source in the crossline direction. Neighboring streamers are separated 75 m from each other, and the receiver separation is 12.5 m. The simulation was made in such a way that it only creates receiver ghost in the data. The configuration of velocity and reflectors are shown in Figure 3.

The 2D method, the implicit 3D algorithm, and the explicit 3D algorithm were tested using this synthetic data. For the 2D method, data were transformed into the time-slowness domain using a 2D high-resolution linear Radon transformation on the streamer, and the deghosting operator was applied in the frequency-slowness domain. To reduce ringing, the amplitude gain of the deghosting operator is limited by 20 dB. Lastly, an inverse linear Radon transformation converts the deghosted frequency-slowness panel back to the time-offset domain together with another Fourier transformation.

The implicit 3D algorithm was applied in the time-offset domain instead of the time-slowness domain as is typically done in production. Each window consists of only one trace, and the length of the window changes with the offset so that it contains only one event. Unlike in the implicit 3D algorithm, the cube size for the explicit 3D algorithm is fixed. Each cube has 5 neighboring streamers and 61 channels from each streamer and extends 1.5 s. Neighboring cubes have some overlap.

We used frequency-dependent reflection coefficient as shown in equation (2), where $r_0 = 0.990$, with parameter $\sigma = 1201.1$ Hz. The reflection coefficient only decreases to 0.987 at 70 Hz.

Figure 4 shows the data before and after deghosting and their spectra from the center streamer. The 2D method failed since it used the wrong ghost delay time, especially for the water bottom. The two deep events were deghosted relatively better, as their incident angle is closer to vertical than the water bottom.

Results are comparable between the implicit and explicit algorithm, while the explicit algorithm shows a few more artifacts. We suspect that the small window size used by the implicit algorithm brings advantages.

**Field WAZ data tests**

The implicit 3D algorithm can be used for source and receiver deghosting at the same time, or individually. Figure 5 presents the comparison of a shot gather before and after deghosting, from a Gulf of Mexico dataset. Both source and receiver side deghosting were applied using the implicit algorithm. The acquisition takes a staggered configuration, as shown in Figure 5c. The crossline distance from the source to streamer is about 2400 m for the tested gun-streamer pair. The offset changes between the neighboring receivers near 90 degree azimuth are so fine that the smallest offset difference from one receiver to its neighbor is about 0.03 m. We used 2D high-resolution linear Radon transformation in the inline direction for each streamer. The source depth is 10 m and the streamer is towed at 12 m deep.

Both the source and receiver side deghosting were applied in the frequency-slowness domain transformed from the common shot gather of each streamer. Shown in Figure 5a and b, the red box encloses a region near the water bottom, while the green box includes its first order multiple. Though they share similar dip in the inline direction with near zero inline slowness, they have different ghost delay times due to different crossline slowness. Using a simple calculation, we know that the first non-zero receiver side notch for the water bottom is around 83 Hz, indicated by the red arrow, and that of the first order multiple, which has a larger ghost delay time, is near 67 Hz, demonstrated by the green arrow. After deghosting, the spectra of the two regions become similar as the notches are correctly filled, as shown in Figure 5e.

The field data shown in in Figures 6 and 7 are from another WAZ acquisition in the Gulf of Mexico. Here we compare three approaches: 2D deghosting, implicit 3D deghosting, and explicit 3D deghosting. We pick two common channel gathers for comparison. One is from a near streamer, which is immediately behind the source and therefore has fewer 3D effects. The other is from a far streamer, which is 2400 m away in the crossline direction from the source. Only receiver deghosting has been applied to simplify the comparison. The acquisition consists of four vessels. Each recording vessel tows 10 streamers 12 m underwater. The streamers are separated by 120 m from each other. The receiver group separation is 12.5 m. The source is at 10 m deep. The water bottom depth ranges from 350 m to 1000 m for the data in this example.

Data from the common shot gather of each streamer were first transformed into the time-slowness domain for the 2D method and the implicit 3D algorithm using a 2D high-resolution transformation. It is assumed that the receivers are uniformly distributed along the streamer with 12.5 m sampling in the transformation. The 2D method was applied on each slowness trace, and the implicit 3D algorithm was applied after dividing the time-slowness panel into overlapping small windows. The depth of each window for the implicit algorithm changes from 1 second for zero slowness, to 0.5 seconds when slowness reaches 0.000667 s/m.

Unlike the other two methods, the explicit 3D algorithm works on common shot gathers involving all 10 streamers. We used a fixed cube size in our implementation. Each cube in this example consists of 4 streamers and 60 channels from each streamer and extends 2 seconds in time. There are overlaps between neighboring cubes. In each iteration, only about 6% of all eligible slowness pairs were incorporated into the second run. The computation was repeated twice to avoid missing weak events.

The same reflection coefficient was used in all three methods, with $r_0 = 0.95$ and $\sigma =$ 240 Hz. At the nominal notch frequency 62.5 Hz, the deghosting operator has about 19 dB gain.

All three methods work well for the near streamer. Figure 6 shows a common channel gather from the selected streamer, with a) from the input data, b) for the 2D method, c) for the implicit 3D method, and d) for the explicit 3D method. The similarity among the three methods proves that the 3D effect is negligible for this data set. Spectra before and after deghosting are shown in Figure 6e for the input data (dark red), 2D method (yellow), 3D implicit method (red), and 3D explicit method (green). It is interesting to note that below about 45 Hz, the three spectra almost overlap each other. After that, the explicit 3D method recovers more energy than the other two until about 70 Hz. Since both the 2D method and implicit 3D method use Radon transformation, we suspect this is caused by the constant receiver depth assumption they use. The explicit algorithm uses the recorded receiver depth in its computation, which has about ±1 m variance.

Strong ringing appears near the water bottom after deghosting using the 2D method for the far streamer. The implicit 3D method takes care of the 3D effects by adaptively changing the delay time, and achieves similar results as the explicit 3D method. Figure 7 presents the test results for the far streamer. The red circle encloses a region where diffractions are mixed with other events. The 2D method behaves worst, showing strong ringing. Though the explicit method does better than the 2D method, it suffers from cross-talk between different events, resulting in noisier output than the implicit method. The implicit method, benefiting from the separation in the time-slowness domain, provides the cleanest result. The bump near 62 Hz in the spectrum of the 2D method is an indication of the ringing near water bottom. Spectra of the implicit and explicit algorithm match relatively well before 50 Hz. After that, the aliasing gradually takes effect.

**Conclusion**

Three-dimensional effects are a major challenge in processing-based deghosting. In this paper, we mainly compared two strategies for deghosting marine seismic data accompanied with 3D effects. The explicit 3D algorithm relies on the sparseness in the slowness domains to reduce aliasing caused by the sparse sampling in the crossline direction. The implicit 3D algorithm, however, utilizes an adaptive algorithm to adjust the ghost delay time to compensate possible 3D effects. In our tests, we have found that both methods provide us with comparable results, and it is difficult to judge which one is better.

The implicit algorithm has no requirement with regards to the crossline sampling. Instead, it assumes minor volatility of ghost delay time in each window. The possibility exists that the assumption may be violated and ringing may appear after deghosting, especially for complex geology. The algorithm is adaptive so it can tolerate measurement errors in the sound velocity and source or receiver depth. Its flow is similar to that of the 2D method. It uses mature techniques and is much easier to apply than the explicit method. The linear Radon transformation effectively separates events according to their dips in the inline direction, but also limits the use of the implicit algorithm to horizontal streamers.

The explicit algorithm uses the receiver depth in its computation and can take advantage of the ghost diversity provided by slant streamers. It partially solves the crossline sampling problem by reducing the range of slowness and applying weighting using information obtained from low frequencies. The sparse sampling in the crossline direction put strains on the explicit algorithm in two ways. Firstly, in the initial run, it lowers the aliasing frequency, reduces the resolution, and makes the slowness picking more difficult. Secondly, in the subsequent run, aliasing becomes harder to avoid when the range of slowness is not small enough. This becomes especially serious for shallow data when the slowness in the crossline direction changes dramatically over a short distance. Though the explicit algorithm is much more computationally intensive than the implicit algorithm, it provides more benefits. By solving the deghosting problem in the time-slowness domain, it can also be used for redatuming, regularization, or even designature at the same time.

Determination of the method to use depends on the data and the user's expectations. The route to improving the deghosting process is also one where assumptions are broken continuously. It is a tradeoff between accuracy and computation complexity. Without the 2D assumption, we can solve the deghosting problem with fewer artifacts, but for the price of a more intense computation.

**Acknowledgements**

We would like to thank TGS for permission to include the Declaration and Justice data in this paper. We also thank the anonymous reviewers as well as the associate editor and Dr. Tijmen Jan Moser for their comments and suggestions. Zhang also wishes to thank Sampad Laha for inspiring discussions and Dr. Guy Hilburn for reviewing the paper.

**References**

Amundsen L. 1992, Wavenumber-based filtering of marine point source data. *62nd Annual International Meeting, SEG, Expanded Abstracts*, 1104-1107

Berkhout A.J. and Blacquiere G. 2015, Deghosting by echo-deblending. *Geophysical Prospecting* **64**(2), 406-420.

Carlson D.A., Long W., Tobti H., Tenghamn R., and Lunde N. 2007, Increased resolution and penetration from a towed dual-sensor streamer. *First Break*, **25** (12), 71-77

Grion S., Telling R., and Barnes J. 2015. De-ghosting by kurtosis maximisation in practice. *85th Annual International Meeting, SEG, Expanded Abstracts*, 4605-4609

Hardwick A., Charron P., Masoomzadeh H., Aiyepeku A., Cox P., and Laha S. 2015, Accounting for sea surface variation in deghosting – a novel approach applied to a 3D dataset offshore West Africa. *85th Annual International Meeting, SEG*, 4615-4619

Jovanovich D.B., Sumner R.D., and Akins-Easterlin S.L. 1983. Ghosting and marine signature deconvolution, a prerequisite for detailed seismic interpretation. *Geophysics*, **48**, 1468-1485

King S. and Poole G. 2015. Hydrophone-only receiver de-ghosting using a variable see surface datum. *85th Annual International Meeting, SEG, Expanded Abstracts*, 4610-4614

Masoomzadeh H. and Woodburn N. 2013. Broadband processing of conventional streamer data-optimized de-ghosting in the Tau-P domain. *75th EAGE Conference & Exhibition incorporating SPE EUROPEC, London, UK, Expanded Abstracts*

Masoomzadeh H. and Hardwick A. 2016. Broadband processing of 3D towed streamer data: a critical analysis of 2D and 3D plane wave decomposition. 86th *Annual SEG International Meeting, Expanded Abstract*, 4746-4750

Monk D. and Byerley G. 2016. What does "broadband" mean to an interpreter. 86th *Annual SEG International Meeting*, *Expanded Abstract*, 5113-5118

Orji O., Sollner W., and UiO, L.J. 2013. Sea surface reflection coefficient estimation. 83rd *Annual SEG International Meeting*, *Expanded Abstract*, 51-55.

Ozbek A., Vassallo M., Ozdemir K., Manen D., and Eggenberger K. 2010. Crossline wavefield reconstruction from multicomponent streamer data: part2 – joint interpolation and 3D up/down separation by generalized matching pursuit. *Geophysics*, **75** (6), WB69-WB85

Ozdemir A., Carprioli P., Ozbek A., Kragh E., and Robertsson J. 2008, Optimized deghosting of over/under towed-streamer data in the presence of noise. *The Leading Edge*, **27**(2), 190-199

Poole G. 2013 Pre-migration receiver de-ghosting and re-datuming for variable depth streamer data. 83rd *Annual SEG International Meeting*, *Expanded Abstract*, 4216-4220

Posthumus B. J. 1993. De-ghosting using a twin streamer configuration. *Geophysical Prospecting*, **41**, 267, 267-286

Rickett J.E., Manen D. J., Loganathan P. and Symour N. 2014.Slanted-streamer data-adaptive deghosting with local plane waves. *76th EAGE Conference & Exhibition*, *Amsterdam, Expanded Abstracts*

Riyanti, C., van Borselen R.G., van den Berg P. M., and Fokkema J. T. 2008. Pressure wave-field deghosting for non-horizontal streamers. 68th *Annual SEG International Meeting*, *Expanded Abstract*, 2652-2656

Robertsson J. and Amundsen L. 2014. Deghosting of arbitrarily depth-varying marine hydrophone streamer data by time-space domain modeling 84th *Annual SEG International Meeting*, *Expanded Abstract*, 4248-4542

Soubaras R. 2012. Pre-stack de-ghosting for variable-depth streamer data *74th EAGE Conference & Exhibition incorporating SPE EUROPEC*, Copenhagen, Denmark, Expanded Abstracts

Telling R., Riddalls N., Azmi A., Grion S., and Williams R. 2014. Broadband processing of west of Shetland data *First Break*, **32** (9), 97-103

Trad D., Ulrych T., and Sacchi M. 2003 Latest views of the sparse Radon transform. *Geophysics*, **68**(1), 386-399

Wang P., Ray S., and Nimsaila K. 2014. 3D joint de-ghosting and crossline interpolation for marine single-component streamer data *84th Annual International Meeting, SEG, Expanded Abstracts*, 3594-3598

Zhang Z., Wu Z., Wang B., and Ji J. 2015. Time variant de-ghosting and its applications in WAZ data *85th Annual International Meeting, SEG, Expanded Abstracts*, 4600-4604

Zhou Z., Cvetkovic M., Xu B., and Fontana P. 2012. Analysis of a broadband processing technology applicable to conventional streamer data. *First Break*, **30** (10), 77-82

**Captions list**

**Figure 1** Amplitude and phase of ghosting and deghosting operators when $r = 1$ (green), $r = 0.95$ (dashed red), and $r(f) = e^{-\frac{1}{\sigma^2}f^2}$ (dash-dot in black) with σ such that $r(100) = 0.84$. Ghost delay time is set to 20 ms and ghost notches are observed at the multiples of 50 Hz, including 0 Hz. a) Amplitude spectra of the ghosting operators; b) phase spectra of the ghosting operator; c) amplitude spectra of the deghosting operator; d) phase spectra of the deghosting operator.

**Figure 2** Calculation of ghost delay time. a) Geometrically, the ghost delay time could be connected with the slowness or incident angle by positioning a mirror receiver/source above the water bottom; b) ghost delay time with respect to $p_x$ in a 2D arrangement, calculated using equation (5) with $d = 15$ m and $v = 1500$ m/s.

**Figure 3** The velocity model used in the synthetic example. The model has three reflectors at 600 m, 1600 m, and 2600 m, respectively. The source is 1500 m away from the streamer in the crossline direction to mimic a WAZ acquisition.

**Figure 4** Data and amplitude spectra for the synthetic data example using the model set up in Figure 3. The distance is measured in the inline direction. a) ghost free data; b) data with receiver ghost; c) deghosted with the 2D method; d) deghosted with the implicit 3D algorithm; e) deghosted with the explicit 3D algorithm; f) amplitude spectrum for the ghost free data; g) amplitude spectrum for the data with receiver ghost; h) amplitude spectrum after deghosting using the 2D method; i) amplitude spectrum after deghosting using the implicit 3D algorithm; j) amplitude spectrum after deghosting using the explicit 3D algorithm. The color of the curve in the spectra figure matches the box color in Figure 4a.

**Figure 5** A shot gather with one streamer of WAZ data before and after deghosting using the implicit 3D algorithm. a) Input data from a gun-streamer pair; b) after both source and receiver side deghosting; c) gun-streamer configuration for the tested shot, the crossline distance from the source to streamer is about 2400 m; d) amplitude spectra before deghosting, the red and green curves show the spectrum within the red and green box, respectively; c) amplitude spectra after deghosting, again with the red and green curves showing the spectrum within the red and green boxes, respectively. The red arrow points to the first non-zero receiver notch of the water bottom, while the green arrow points to that of the first order multiple.

**Figure 6** Comparison of the deghosting results using a common channel gather from a near streamer, which is directly behind the source. a) Input data; b) after receiver side deghosting using the 2D method; c) using the implicit 3D deghosting algorithm; d) using the explicit 3D deghosting algorithm; e) spectra of the input (dark red), 2D method (yellow), and the implicit (red) and explicit algorithm (green); f) positions of the source and streamer. Spectra are plotted using the whole data set.

**Figure 7** Comparison of the deghosting results using a common channel gather from a far streamer, which is 2400 m away from the source in the crossline direction. a) Input data; b) after receiver side deghosting using a 2D method; c) using the implicit 3D deghosting algorithm; d) using the explicit 3D deghosting algorithm; e) spectra of the input (dark red), 2D method (yellow), and the implicit (red) and explicit algorithm (green); f) positions of the source and streamer. Spectra are plotted using the whole data set.

Figure 1

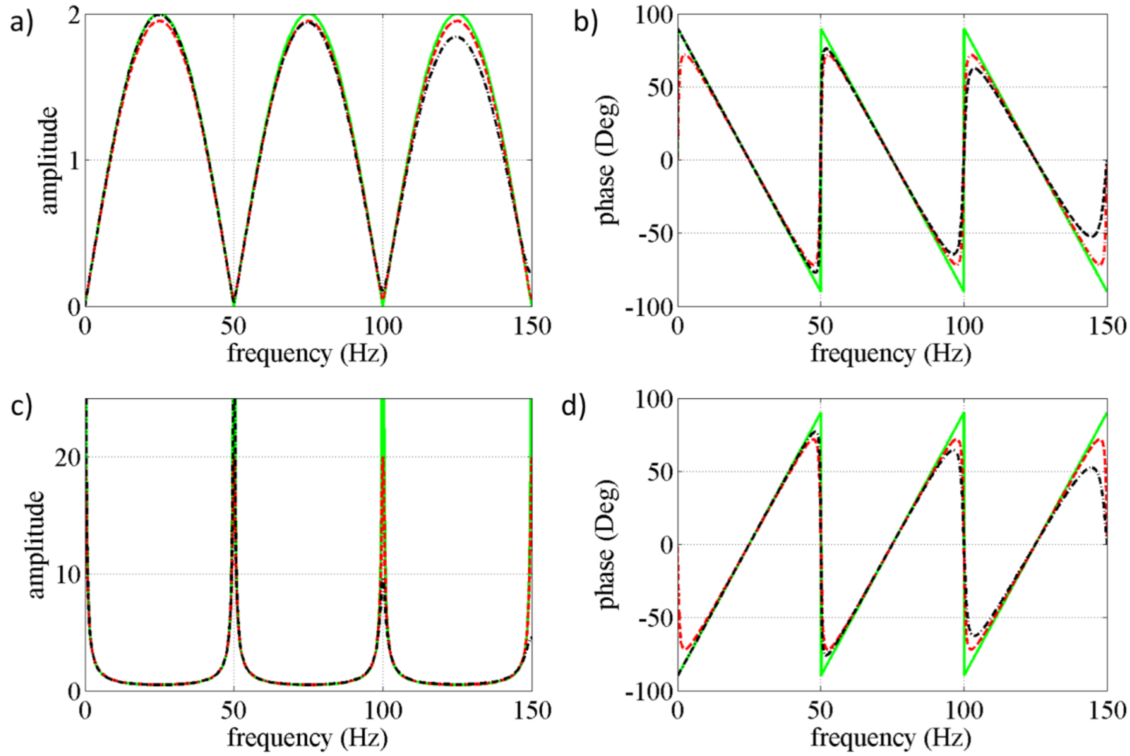

a)
amplitude
frequency (Hz)
b)
phase (Deg)
frequency (Hz)
c)
amplitude
frequency (Hz)
d)
phase (Deg)
frequency (Hz)

Figure 2

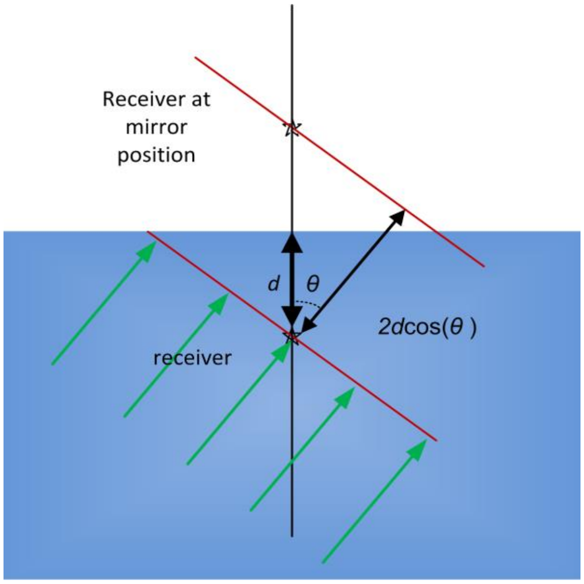
Receiver at
mirror
position
d
θ
2dcos(θ )
receiver

a)

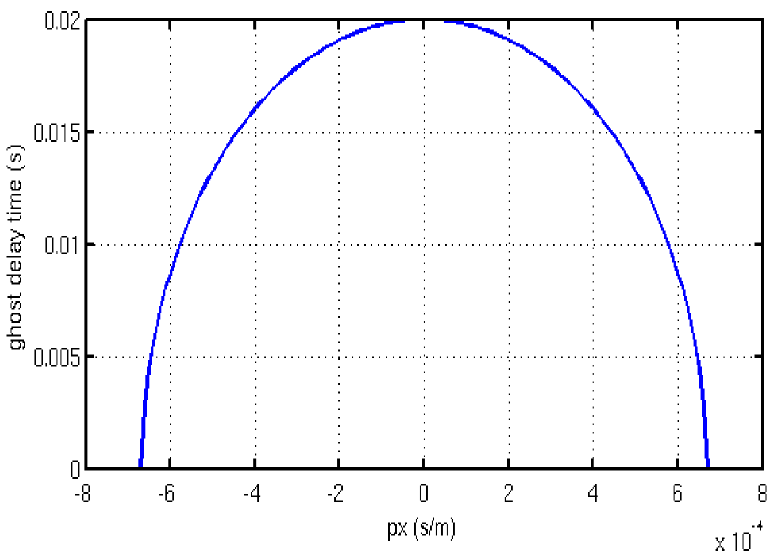
0.02
0.015
0.01
0.005
0
ghost delay time (s)
-8
-6
-4
-2
0
2
4
6
8
px (s/m)
x 10^-4

b)

Figure 3

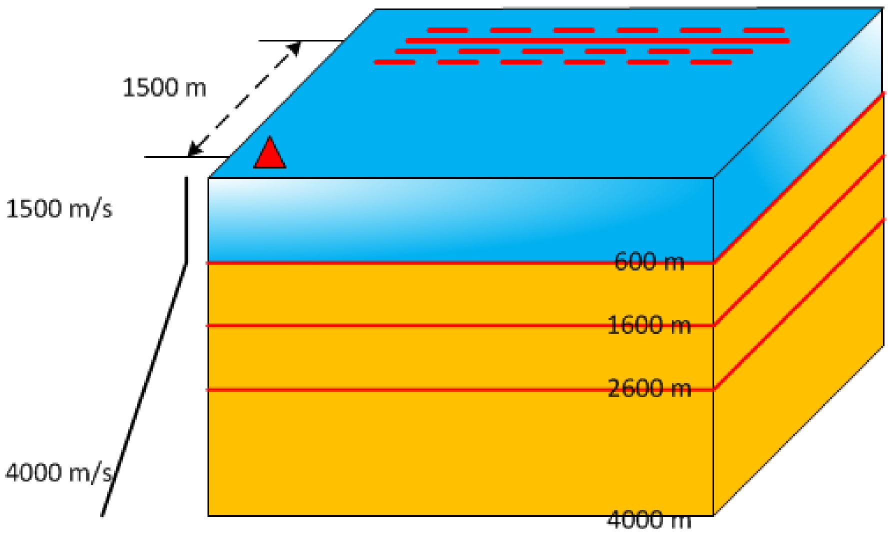

Figure 4

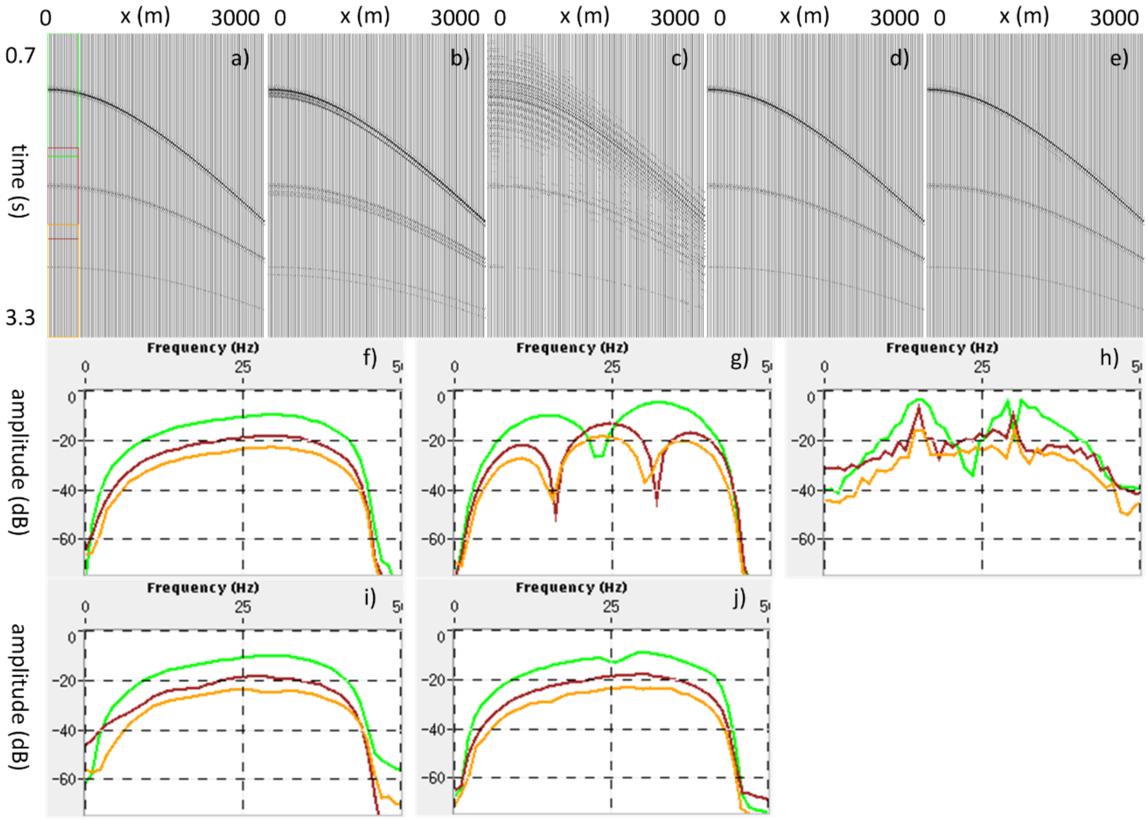

0
x (m)
3000
0.7
time (s)
3.3
a)
b)
c)
d)
e)
Frequency (Hz)
0
25
amplitude (dB)
-20
-40
-60
f)
g)
h)
i)
j)

Figure 5

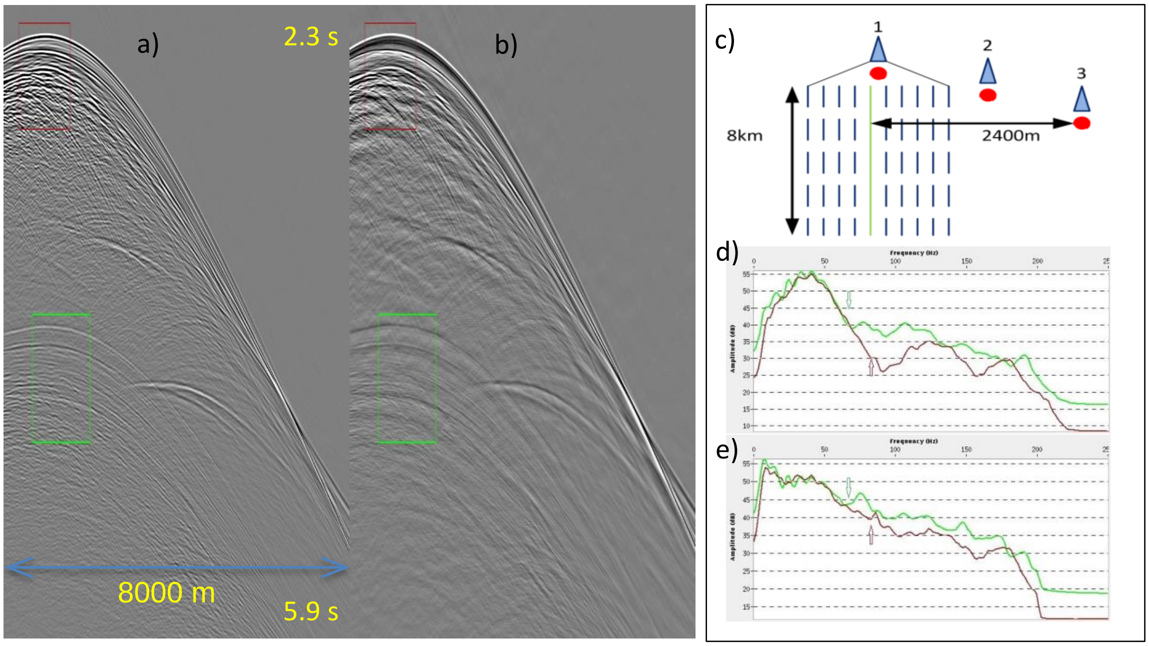

Figure 6

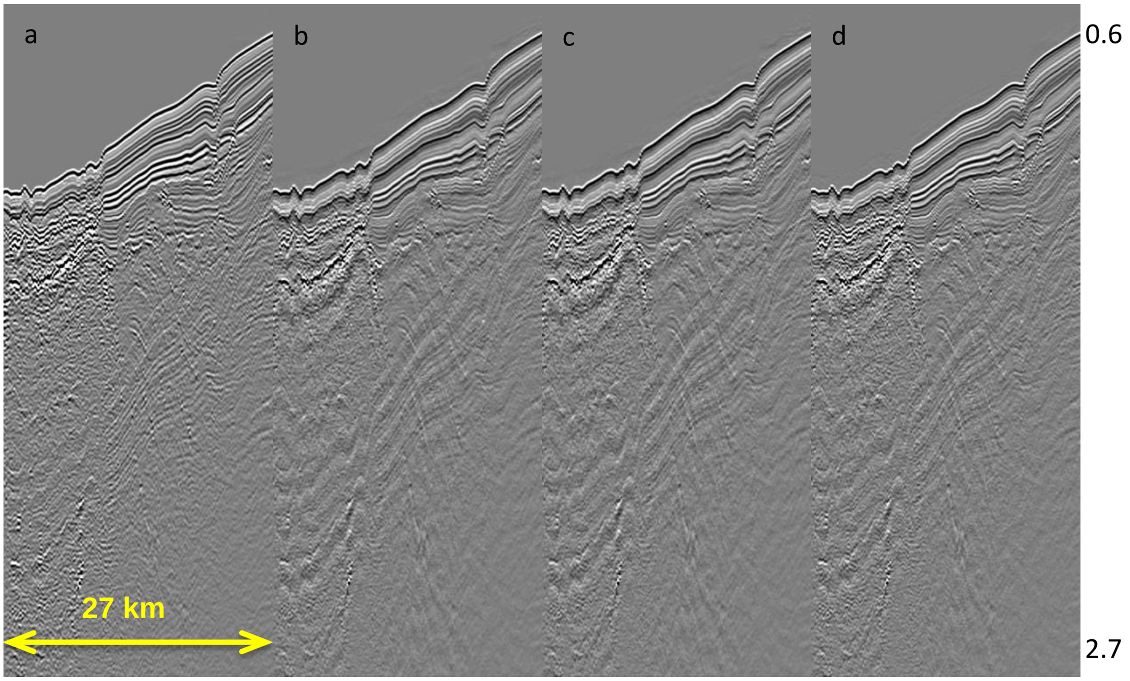

a
b
c
d
0.6 s
27 km
2.7 s


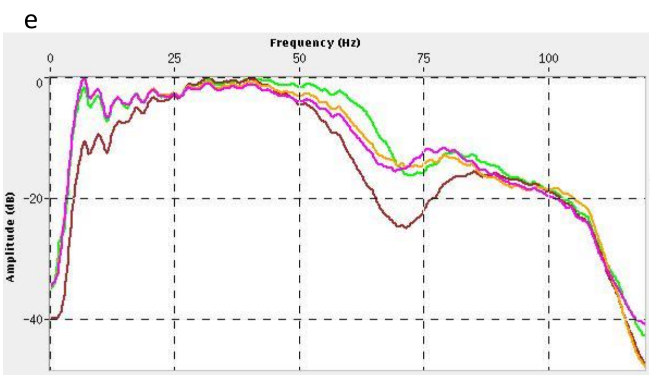

e
Frequency (Hz)
0
25
50
75
100
Amplitude (dB)
0
-20
-40


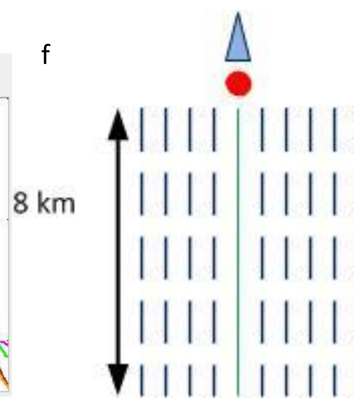

f
8 km

Figure 7

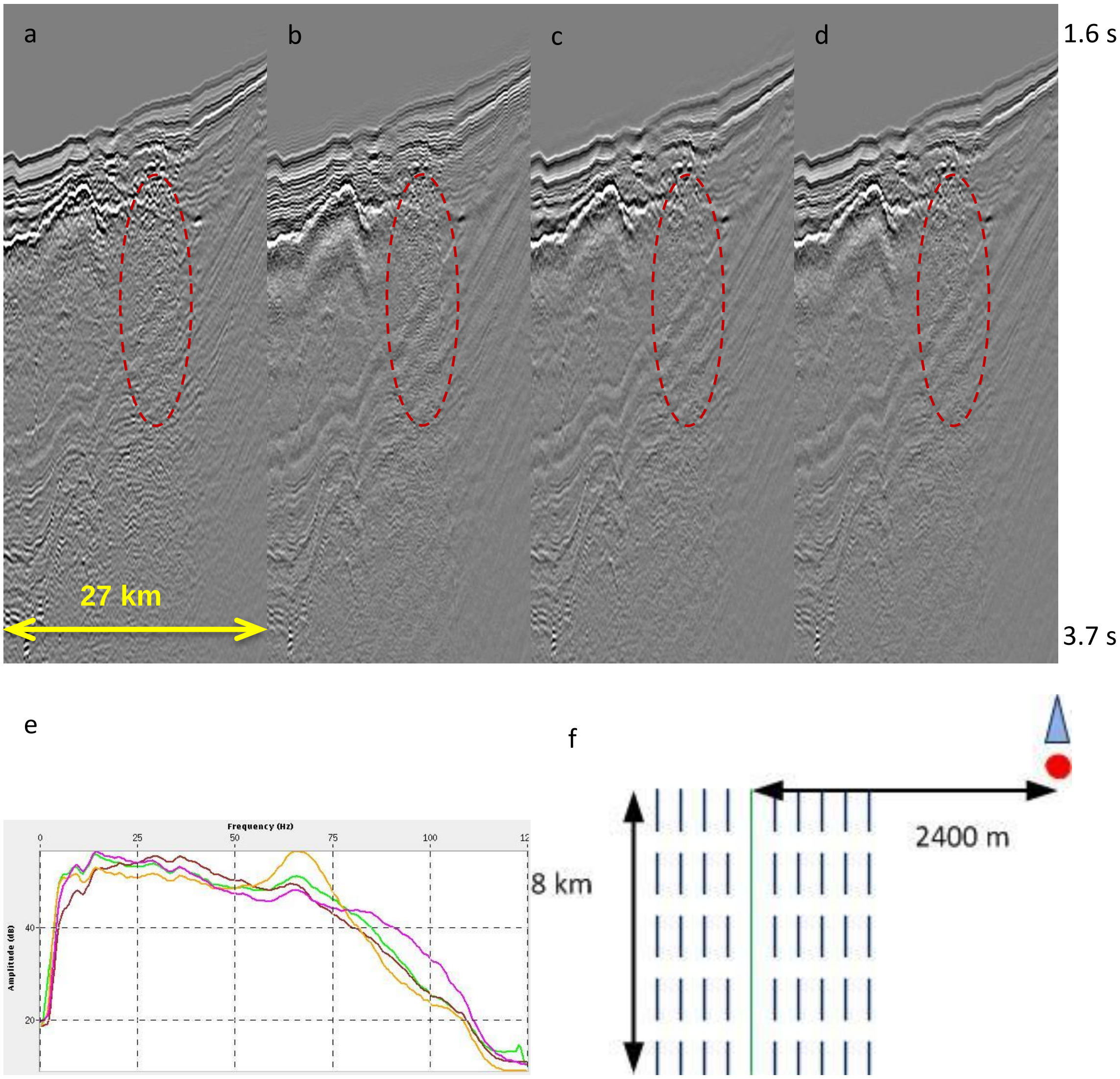
a
b
c
d
1.6 s
27 km
3.7 s
e
Frequency (Hz)
0
25
50
75
100
Amplitude (dB)
40
20
f
8 km
2400 m